Integrin adhesion drives the emergent polarization of active cytoskeletal stresses to pattern cell delamination

C. Meghana[a], Nisha Ramdas[b], Feroz Meeran Hameed[b], Madan Rao[b,c], G. V. Shivashankar[b,d], and Maithreyi Narasimha[a,1]

[a]Department of Biological Sciences, Tata Institute of Fundamental Research, Mumbai 400005, India; [b]National Center for Biological Sciences, Bangalore 560065, India; [c]Raman Research Institute, Bangalore 560080, India; and [d]Mechanobiology Institute and Department of Biological Sciences, National University of Singapore, Singapore 117411

Edited by James A. Spudich, Stanford University School of Medicine, Stanford, CA, and approved April 13, 2011 (received for review December 14, 2010)

Tissue patterning relies on cellular reorganization through the interplay between signaling pathways and mechanical stresses. Their integration and spatiotemporal coordination remain poorly understood. Here we investigate the mechanisms driving the dynamics of cell delamination, diversely deployed to extrude dead cells or specify distinct cell fates. We show that a local mechanical stimulus (subcellular laser perturbation) releases cellular prestress and triggers cell delamination in the amnioserosa during *Drosophila* dorsal closure, which, like spontaneous delamination, results in the rearrangement of nearest neighbors around the delaminating cell into a rosette. We demonstrate that a sequence of "emergent cytoskeletal polarities" in the nearest neighbors (directed myosin flows, lamellipodial growth, polarized actomyosin collars, microtubule asters), triggered by the mechanical stimulus and dependent on integrin adhesion, generate active stresses that drive delamination. We interpret these patterns in the language of active gels as asters formed by active force dipoles involving surface and body stresses generated by each cell and liken delamination to mechanical yielding that ensues when these stresses exceed a threshold. We suggest that differential contributions of adhesion, cytoskeletal, and external stresses must underlie differences in spatial pattern.

cell extrusion | cell mechanics | tissue dynamics | wound-healing

The establishment and maintenance of tissue pattern depends on cellular interactions mediated predominantly by the cadherin and integrin families of adhesion molecules. Their coupling to the (active) cytoskeleton enables mechanochemical transduction and through it the ability of cells in dynamic epithelia to actively generate, transmit, and sense mechanical stresses (1–4). How mechanochemical transduction is spatiotemporally regulated to facilitate the complex and diverse spatial patterns of tissues is poorly understood.

The amnioserosa (AS) during dorsal closure in *Drosophila* provides a rich heterogeneity of patterned cell behaviors and an attractive in vivo model to address the interplay between adhesion, active forces, and cell behavior. Genetic and large-scale laser perturbations have shown that it is the principal driving force for dorsal closure (5–8). Its contraction by apical constriction [at ≈2 μm^2/s during mid to late dorsal closure (5)] over the yolk cell helps establish continuity of the epidermis through the meeting of the leading edge cells of the epidermis to which it is bound (6, 7, 9). A small fraction of AS cells is also extruded seemingly stochastically from the epithelium (delamination) without compromising its integrity and is necessary for the timely completion of dorsal closure (9, 10). What underlies this stochasticity and how it is accommodated within the stereotypical dynamics of the AS remain unclear. Because delamination is commonly used to eliminate dead cells or to single out cells to adopt distinct fates, and is misregulated in cancers, an understanding of its patterning principles is of general interest.

Here we show that a local mechanical stimulus delivered through controlled subcellular cytoplasmic laser perturbations (11, 12) can induce delamination that, at later times, qualitatively and mechanistically recapitulates the approach to natural/spontaneous delamination. We use this in combination with high-resolution 4D confocal microscopy, genetic perturbations, and quantitative morphological analysis to investigate the molecular correlates for active stress generation and transmission underlying the dynamics of cell delamination in the AS. We delineate the timeline of cellular and cytoskeletal remodeling events, produce a time-dependent strain map, estimate cellular prestress, and study their regulation. We suggest that the dynamics of strain patterning including the threshold dynamics of delamination can be modeled on the basis of active gels, which incorporates the generation and response of active stresses arising not only from contractile cell surface stresses (13, 14) but also cell-body stresses (15, 16).

Results

Subcellular Cytoplasmic Laser Perturbation Releases Prestress and Triggers Cell Delamination. We focus on single central AS cells (DC; Fig. 1*A*) during early dorsal closure (when the contribution from boundary stresses can be ignored) and target the laser to a diffraction-limited spot in the cytoplasm (cytoskeletal structures), midway between the plasma membrane and the nucleus and 2 μm basal to the apicolateral membrane visualized by E-Cadherin GFP. We use pulse energy regimes (1.7–2 nJ) previously reported to create local but not collateral damage (*Materials and Methods* and ref. 17) and ensure the integrity of the plasma membrane, unlike the hole-drilling experiments described elsewhere (18–21). The nature of mechanochemical coupling of AS cells through adhesion molecules is depicted in Fig. 1*B* (7). The contractile stress that stabilizes cell–cell interfaces and holds cells together is called the prestress, an immediate consequence of the active state of the cell due to microscopic stresses generated in the actin and microtubule cytoskeletons. As a consequence, every cell–cell interface must satisfy force balance.

Upon perturbation, the nucleus shrinks, confirming that it disrupts the cytoskeletal meshwork of the targeted cell (Fig. S1*A*) (11). Like the recoil of wound edges resulting from cell loss in tissue scale laser ablations (6), the DC expands, despite the absence of a real "wound" (Fig. 1 *D1* and *D2* and Movie S1), strengthening the idea that prestress and the expansion resulting from its release are manifestations of the constraints imposed by mechanical springs that link the membrane and the nucleus (22). This consistently results in its delamination from the layer, suggesting an imbalance of forces at the DC–nearest neighbor (NN) interface. Viewing the tissue as a closely packed collection of

Author contributions: C.M., G.V.S. and M.N. designed research; C.M., N.R., and M.N. performed research; C.M., F.M.H., and M.N. contributed new reagents/analytic tools; M.N. conceived of the study; M.R. contributed the theory; C.M., M.R., G.V.S., and M.N. analyzed data; and C.M., M.R., G.V.S., and M.N. wrote the paper.

The authors declare no conflict of interest.

This article is a PNAS Direct Submission.

[1]To whom correspondence should be addressed. E-mail: maithreyi@tifr.res.in.

This article contains supporting information online at www.pnas.org/lookup/suppl/doi:10.1073/pnas.1018652108/-/DCSupplemental.

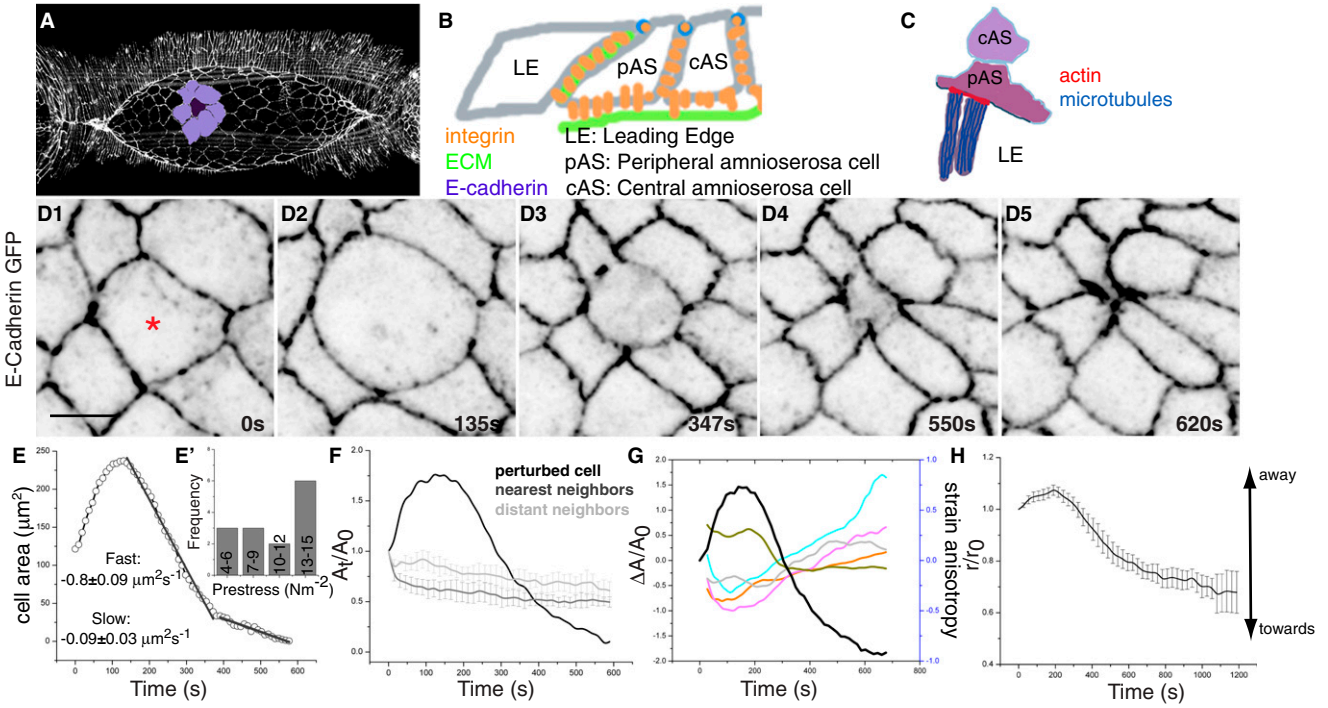

Fig. 1. Cellular dynamics associated with subcellular cytoplasmic laser perturbation. (*A*) Stage 14 embryo showing the contour of the AS highlighting a cohort of cells with the delaminating cell (DC, purple) surrounded by its nearest neighbours (lilac). Schematic representation of the adhesive interfaces that enable cellular interactions in the AS (*B*) and cytoskeletal organization at the LE–pAS cell interface (*C*). (*D1–D5*) Time-lapse confocal images of an embryo labeled with E-Cadherin GFP. (*E*) Representative graph of apical surface area dynamics showing typical velocities (mean ± SEM) of constriction (n = 5). (*E′*) Frequency distribution of prestress. (*F*) Fractional change in apical surface area of DC (black), its NN (dark gray, n = 5), and DN (light gray, n = 4). (*G*) Strain anisotropy of NN (colored) and apical surface area of the DC (black). (*H*) Centroid position of the NN with respect to the DC (n = 9). Asterisks indicate perturbed cell. Analysis of fractional change in area and perimeter, strain anisotropy, and circularity changes of multiple cohorts can be found in Fig. S1. (Scale bar, 10 μm.)

"deformable cells" (without voids), we study morphological distortions and displacements of cells accompanying induced delamination (*SI Text*, *Theoretical Considerations*, *Sequence of symmetry breaking shape transitions before delamination*). Immediately upon its perturbation, the DC expands isotropically (as measured by circularity; Fig. S1*E*) for up to 200 s to twofold its initial area (Fig. 1*E* and Fig. S1 *B1–D1* and *B2–D2*) along the radial direction (at ≈0.8 μm²/s). During this time the centroid positions of the DC remain unchanged. Its area then reduces exponentially toward ultimate delamination, complete in ≈10 min after induction (Fig. 1 *D2–D5* and *E–G* and Fig. S1 *B1–D1*). A two-piece linear decomposition allows the parsing of the contraction phase into an early fast phase (0.8 ± 0.09 μm²/s; n = 5) and a late slow phase (0.08 ± 0.03 μm²/s; n = 5; Fig. 1*E*). An abrupt decrease in area with increasing circularity and rates similar to the slow phase (0.06 ± 0.006 μm² s^{-1}; n = 15) but not preceded by expansion accompanies natural delamination (Figs. S2 *A1–D1*, *A2–D2*, *E*, and *F* and S3 *A–C*).

We use the linear, early (<200 s) isotropic expansion in cell area (A) to obtain a quantitative estimate of the prestress $\sigma^{(\mathrm{pre})}$ using $A \approx \frac{2\pi d^2 \sigma^{(pre)}}{\eta}$, where d is the cortical thickness and η the cytoplasmic viscosity (*SI Text*, *Theoretical Considerations*, *Estimation of cellular prestress* provides a description of this derivation). If we assume that dissipation of this force occurs between AS cells at these timescales (23), η =1 Pa s (24) and $_d$ ≈100 nm (25), then the distribution of slopes from this initial expansion phase gives a narrow distribution of prestress, typically on the order of 12–15 N m^{-2} (Fig. 1*E′*) and at the lower end of the range of magnitudes reported elsewhere (26).

Perturbation Induces Local Spatial Pattern: Rosettes and Asters. Upon perturbation, the NN cells of the DC initially squeeze along the radial and expand along the azimuthal direction, creating an anisotropy in shape (i.e., $S_A < 0$ with little or no change in apical surface area) (Fig. 1 *D2* and *F–G* and Fig. S1 *B1–D1* and *B3–D3*; *SI Text*, *Theoretical Considerations*, *Sequence of symmetry breaking shape transitions before delamination*). After maximum expansion of the DC, the shape anisotropy in the NN cells changes sign ($S_A > 0$) as they actively shrink in the azimuthal and elongate in the radial direction (Fig. 1 *D3–D5* and *G* and Fig. S1 *B3–D3*), reinforcing the rosette. Large directional displacements of the NN cells mark the onset of delamination. This is evident from their centroid displacements whose velocity vectors point radially into the centroid of the DC (we refer to this pattern as asters; Fig. S4 *A–C*) and is reflected in the dynamics of the radial distance between the centroids of the DC and NN cells (Fig. 1*H* and Fig. S4*D*). Similar shape transformations ($S_A > 0$; Figs. S2 *A3–D3* and S3*A* and Movie S7) and centroid displacements (Figs. S4*B* and S3*D*) accompany natural delamination. In both cases, distant neighbors (DN) of the DC do not display significant systematic displacement or deformation, suggesting that the patterning induced by delamination is limited to a cohort including NN cells and that the stresses generated do not propagate very far and are "screened" over a length of two cell diameters. We next address the basis for the deformation and displacement dynamics by probing the dynamics of the cytoskeleton.

Emergent Polarization of Cytoskeletal Elements Generates a Hierarchy of Active Stresses. We find a consistent pattern of deployment of cytoskeletal elements, suggesting a temporal hierarchy of active force generators (Fig. 4 *A* and *B* and *Discussion* for typical times and regimes). The first observable change (<60 s upon perturbation) is the flow of myosin (sqhGFP) in the NN as directed particulate streams toward each DC–NN interface (Fig. 2 *A1–A4* and Movie S2), leading to its enrichment in the apical plane (Fig. 2 *A5–A8*). Nearly concomitantly, actin-rich lamellipodia from the apical membranes of NN cells grow into the DC from all sides,

with their trailing edge at the DC–NN interface (Figs. 2 *B1* and *B2* and 3 *D1* and *D2* and Movie S3) as the area of the DC reduces (Figs. 2*B* and 3*D*). During this time, actin accumulates at the DC–NN interface to form an actin collar with progressive apical constriction of the DC (Figs. 2*B3* and 3 *D2* and *D3*). These changes occur in the NN, evident from their presence even when the DC is not GFP positive (Fig. 2*B* and Movie S4). After this, the microtubules become enriched at the DC–NN interface with their plus ends (EB1 GFP) directed toward it (Fig. 2*C*, Fig. S5 *A* and *B*, and Movie S5). In the DC, however, there is a loss of actin, myosin, and microtubules (Figs. 2 *A4* and *C2* and 3*D2*, Fig. S5 *A3*, *B1*, and *B4*, and Movies S2, S3, and S5). Cytoskeletal rearrangements in NN cells that include directed flows of myosin (in the bulk) and actin (200 s before extrusion) leading to the formation of a cortical actomyosin collar at the DC–NN interface, the polarization of apical microtubule meshwork, and their depletion in the DC also characterize the cytoskeletal response to natural delamination (Fig. S3 *E–I* and Movies S8–S10). A striking feature of both is their polarization in the NN toward the DC and their loss in the DC, suggesting that delamination may be driven by a force imbalance, with the net force vector pointing into the DC. The directed movement of actin, myosin, and microtubules in the NN, like their displacements, also forms aster-like patterns.

Adhesion at Cellular Interfaces Directs the Emergence of Cytoskeletal Polarities and Modulates Mechanical Impedance and Delamination Dynamics. The influence of laser perturbations on the NN prompted us to ask whether adhesive interactions at cellular interfaces were necessary. We have previously shown that the molecular composition of the leading edge (LE)–peripheral AS cells (pAS) interface is different from other pAS cell interfaces with respect to the nature of integrin interactions (Fig. 1*B*) (7). That these differences in adhesion are critical determinants of pAS cell behavior is evident from the phenotypes observed in integrin mutants: whereas wild-type pAS cells constrict anisotropically and ahead of the central AS cells, mutant cells elongate/expand (7). Consistent with this, we find that subcellular perturbation in the pAS cell results in its anisotropic expansion characterized by poor or no expansion at the interface with the leading edge but expansion at all other interfaces, as indicated by the dynamics of shape anisotropy (Fig. 3*A*; *Materials and Methods*). This suggests that the mechanoresponse to perturbation is sensitive to native local anisotropies in adhesion.

We next examined the effect of reduction of the βPS or αPS3integrin subunits known to be functional in mediating adhesion in the AS (Fig. 1*B*) (7, 27). This resulted in altered responses characterized by an increase in the magnitude and duration of the maximally expanded state as well as a significant delay in cell extrusion (Fig. 3*B* and Table S1). To address the basis of the altered dynamics, we examined actomyosin reorganization in these embryos. In both, the lamellipodia that formed in the expansion phase were nonprogressive, more spiky, and seen to grow into both sides of the DC–NN interface (Fig. 3 *D* and *E*, Fig. S6, Table S2, and Movie S6). Although cortical enrichment of actin was evident in the expansion phase in both genotypes, this enrichment disappeared as the cell contracted when βPS but not αPS3 was dowregulated (Fig. 3*E*, Fig. S6, and Movie S6). The directional streaming of myosin and its enrichment at the DC–NN interface were both delayed and reduced (Fig. 3 *F* and *H*). Thus, the emergent polarization of actomyosin structures depends on integrin adhesion, consistent with the altered early dynamics in mutants.

To determine whether the observed microtubule polarization was necessary, we induced delamination in embryos in which microtubules were severed by overexpression of spastin. We observed a modestly reduced expansion response and a significant delay in cell extrusion resulting from a slower second phase, despite nearly wild-type rates of contraction in the first phase (Fig. 3*C* and Table S1). Further, the early, directed, particulate streaming of myosin toward the DC–NN interface was reduced or absent, resulting in a significant delay in its cortical enrichment (Fig. 3 *F* and *G* and Table S1). These results suggest dual roles for the microtubule cytoskeleton: in the DC and in the NN and in the regulation of transport and (through it) in force generation.

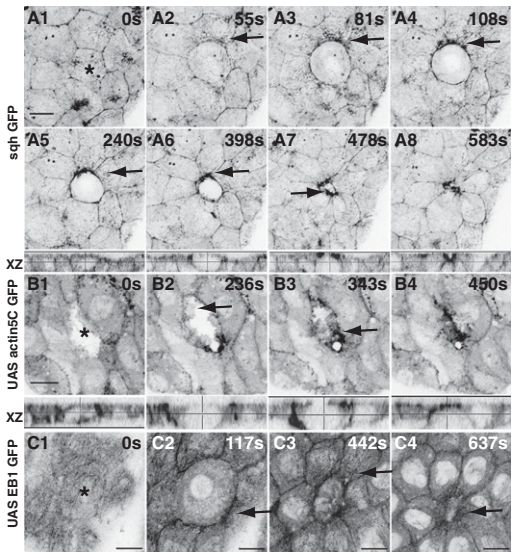

Fig. 2. Emergent polarization of the cellular cytoskeleton in response to subcellular laser perturbation. Time-lapse confocal images of sqhGFP (*A1–A8*), actin5CGFP (*B*), and EB1GFP (*C*) to show actin, myosin, and microtubule dynamics upon perturbation. Arrows point to particulate streams of sqh (*A1–A4*), enrichment at the DC–NN interface (*A5–A8*), actin ruffles in the neighboring cells (*B*; the ablated cell is actin GFP negative), and polarized microtubule reorganization (*C*). Apical projections and orthogonal (XZ) views are shown. Asterisks indicate the ablated cell. See Fig. S5 for response to perturbation of tubulin GFP and microtubule organization in fixed ablated embryos. (Scale bars, 10 μm.)

Discussion

Our explorations of the interplay between molecular processes and physical forces that drive delamination in the AS have shown that it is regulated by an elaborate feedback between the state of individual cells and their collective organization through the generation and propagation of stress and mechanochemical transduction that is dependent on adhesion. We have identified the spatiotemporal sequence of both molecular and physical events (Fig. 4 *A* and *B*; *SI Text*, *Theoretical Considerations*, *Sequence of symmetry breaking shape transitions before delamination*) that contribute to active force generation and transmission of stresses leading to delamination and provide evidence for the emergence of geometric, cytoskeletal, and mechanical polarities. We establish the utility of subcellular perturbations in predicting the contribution of molecules to the dynamic force balance at cellular interfaces during morphogenesis and to the spatial patterning of tissues. We suggest that the dynamics of tissue shrinkage in the AS that includes mechanical yielding beyond a threshold stress can be studied using a theoretical framework based on active hydrodynamics (*SI Text*, *Theoretical Considerations*, *Theoretical proposal based on active hydrodynamics*).

Temporal Ordering of Molecular and Physical Events That Pattern the Dynamics of Delamination. Our work has delineated the temporal hierarchy of cellular rearrangements and deformations, force generators, and transducers that accompany cell extrusion. They show that the dynamics of delamination is patterned locally and is driven by deformations and displacements in a cohort of cells, including the DC and NN, that undergo a sequence of symmetry-breaking shape transitions from nearly circular to elliptical cells ($S_A > 0$) (*SI Text*, *Theoretical Considerations*, *Sequence of symmetry breaking shape transitions before delamination*), creating a rosette pattern around the delaminating cell, which remains isotropic ($S_A = 0$). These shape distortions rely on distinct

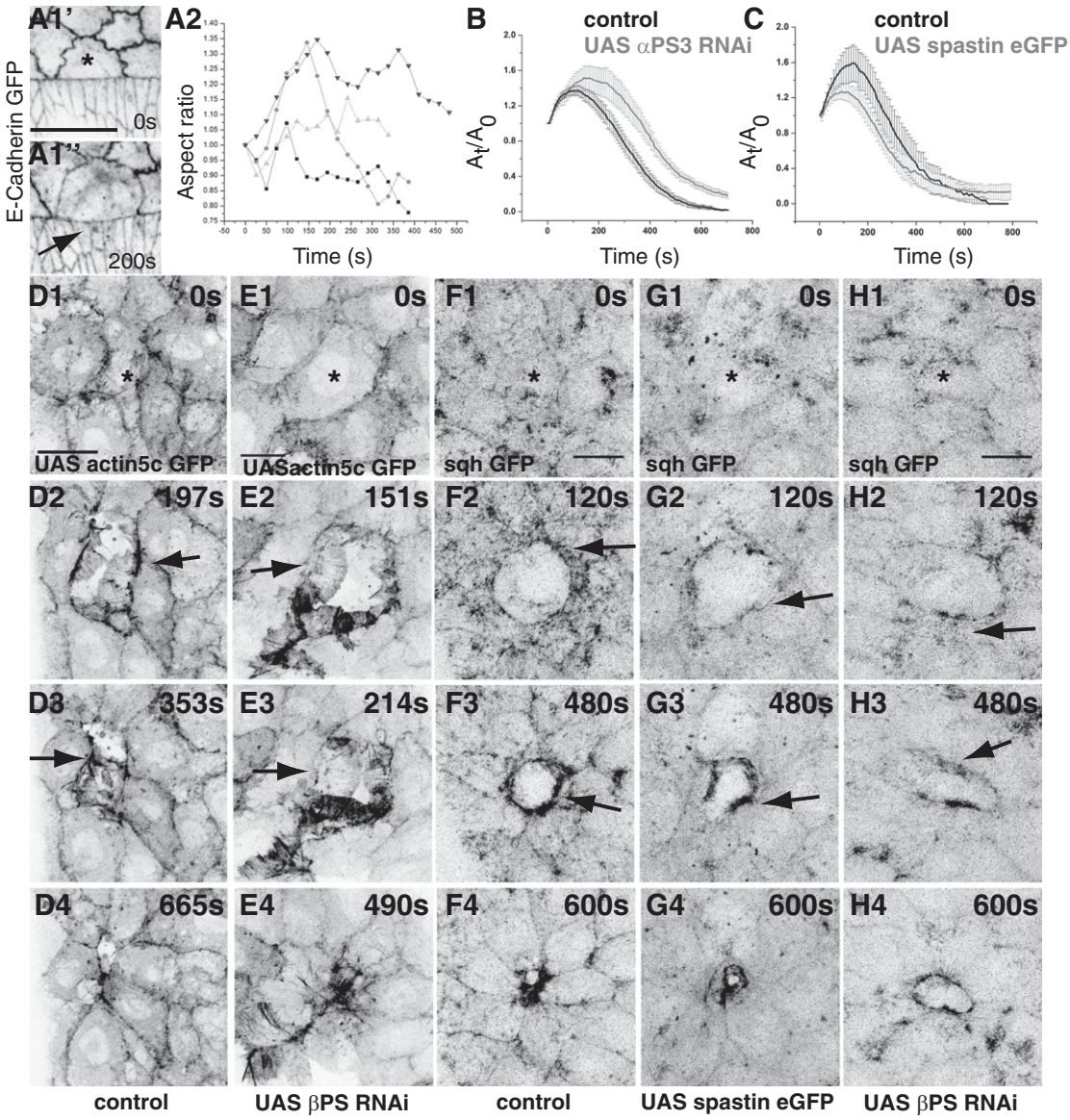

Fig. 3. Adhesion-dependent mechanical compliance and cytoskeletal polarization. Time-lapse confocal images of an embryo labeled with E-Cadherin GFP showing anisotropic expansion (*A1*, arrow; $n = 5$) and aspect ratio dynamics of pAS cells upon perturbation (*A2*). Dynamics of fractional change in apical surface area induced by perturbation in control cells (black in *B* and *C*) and upon expression (gray) of αPS3 RNAi (*B*; $n = 8$) or spastin (*C*; $n = 8$). Time-lapse confocal images showing response of actin (*D* and *E*) and myosin (*F–H*) to cytoplasmic perturbation in control (*D* and *F*), βPS RNAi (*E* and *H*), and spastin-overexpressing embryos (*G*). Asterisks mark perturbed cell. Response of actin to perturbation in αPS3 RNAi can be found in Fig. S6. (Scale bars, 10 μm.)

rearrangements of actin and microtubules that we show here are generated in the neighboring cells in a precise spatiotemporal sequence that can be clustered into five regimes (Fig. 4 *A* and *B*). The dynamics of natural and induced delamination are similar in regimes III–V. Changes in regime I, which herald the response to ablation, are not evident in natural delamination and most likely account for the lower areal velocities comparable to the slow phase of induced delamination. Importantly, these changes, notably directed myosin flows, represent the earliest response to a mechanical stimulus identified in vivo. We think that this leads to the buildup of myosin at the base of the lamellipodium, to fuel its contractility cycles that drive movement of the leading edge (28) to constrict the larger apical surface generated during laser perturbation. Further, the comparison of the deployment of force generators in the two cases suggests that (*i*) during natural delamination the actin collar is programmed to precede microtubule loss in the delaminating cell, so as to prevent the inevitable cell expansion; and (*ii*) myosin flows and lamellipodia-driven motility presumably triggered by expansion contribute to rapid extrusion upon laser ablation. These differences may reflect responses to qualitatively or quantitatively different stresses. The anisotropy in cortical tension, actin contractility (resulting in the actin collar), and polarized microtubules generated in the neighbors in both cases constitute the microscopic generators of the force dipoles associated with each cell. These dipoles are directed radially inward in the form of an aster, get progressively better defined, and account for the finite radial centroid velocity with respect to the substrate to result in contraction of the delaminating cell leading to its ultimate extrusion. The polarization of active stresses in the NN and their loss in the DC tilt the force balance at the DC–NN interface, causing the DC to "yield." Our results suggest that the microtubule cytoskeleton also contributes indirectly to the force balance by enabling the early, polarized transport of myosin. Our work documents the nature, dynamics, multiple modes of organization, and precise spatiotemporal sequence of force generators and their contri-

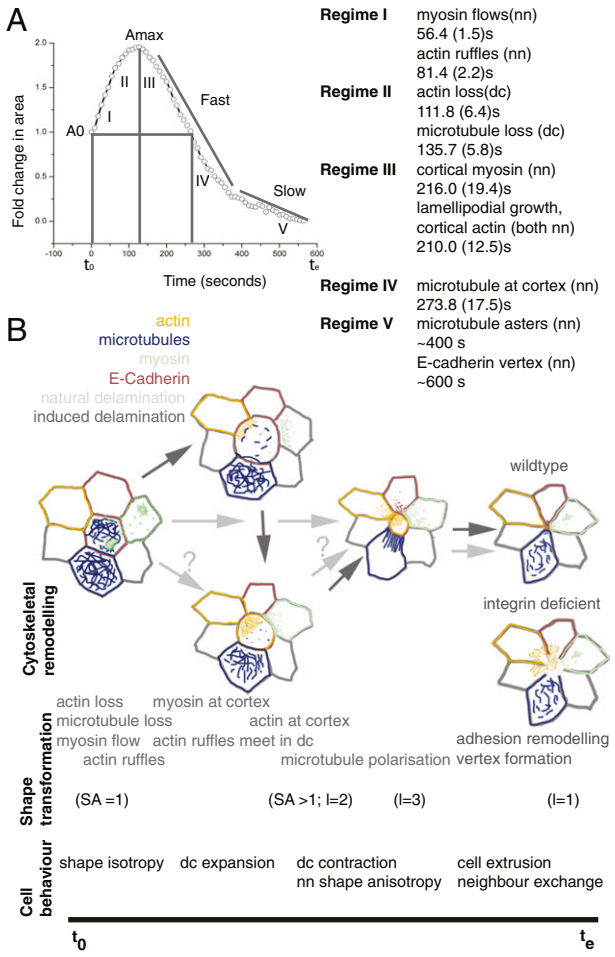

Fig. 4. Temporal hierarchies of molecular and physical events during natural and induced delamination. Schematic representations of cell area dynamics, shape transformations, cytoskeletal dynamics, and cell behaviors that accompany induced (*B*, dark gray arrows) and natural delamination (*B*, light gray arrows) in wild-type embryos are depicted along the timeline beginning at t_0, marking the onset of induction, and t_e, marking the time of cell extrusion; delaminating cell is at the center of the rosette in all images. An integrin-deficient rosette is shown below it. The times of onset from t_0 at which the regimes that characterize the dynamics (*A*, *Right*) become evident are expressed as means computed from multiple movies (numbers in brackets are SEs of mean; n = 8 for actin, 6 for microtubules, and 5 for myosin) and their relation to changes in area that accompany induced delamination (*A*, *Left*). A_0 and A_{max} are initial and maximally expanded normalized areas.

bution to delamination, uncovering its complex regulation, not previously appreciated (21, 29, 30).

Emergence of Cytoskeletal and Mechanical Polarities: A Role for Mechanical Stimuli and Adhesion. A striking feature of all of the cytoskeletal rearrangements we observe (myosin streams, lamellipodial curtains, actomyosin collars, and microtubule asters, in order of appearance; Fig. 4) is their polarization resulting in an overt emergent polarity at the DC–NN interface. They can be described as a sequence of symmetry-breaking steps (31) that result in the collective emergence of polarity. Our results show that this polarity can be induced by an isotropic mechanical stimulus and serves to accomplish the collective shrinkage of a subset of cellular interfaces. Mechanical forces have been shown to trigger actin polymerization in vitro and recruit myosin (32–35). Understanding the nature of mechanical inputs and the molecular flow of information upon mechanical stimulation to specific cytoskeletal force generators to culminate in the emergence of polarity and pattern promises to be an exciting area of inquiry. The spatiotemporal sequence and the collective utilization of the cytoskeletal elements in all NN, notably the precedence of actin over microtubules and their polarization predominantly in the apical plane to generate supracellular structures, resembles what has been observed at the AS–LE boundary (Fig. 1*C*) (9, 36). In both cases, the cell(s) on one side of the interface (DC in the former and pAS cell in the latter) contracts rapidly, whereas the cells on the other side (NN and LE cells, respectively) collectively produce "supracellular" structures that shrink. We speculate that this order ensures contraction by preventing expansion and facilitates the rapid progression of delamination and dorsal closure.

Our work presents several lines of evidence to demonstrate that the response to this mechanical stimulus can be modulated by cell adhesion. Thus, integrins (or cadherins) on the apicolateral membrane (7) of the AS may serve as mechanosensors and signal specific reorganization of the actin (and microtubule) cytoskeleton. Our results also argue that whereas differences in adhesion are genetically hardwired to generate a spatiotemporal pattern at the AS–LE boundary, differences at the DC–NN interface must emerge spontaneously, presumably in response to a local mechanical stress. Understanding the nature of these differences will be interesting to pursue. Further, given the nature of the inducing mechanical stimulus (noninvasive, nanoscale), we speculate that responses to wounding may also be triggered primarily by a mechanical stimulus rather than the loss of membrane/tissue integrity.

It has been previously argued that an apoptotic signal triggers delamination (10). Our analysis of natural and induced delamination (Fig. S5 *C* and *D*) reveal that in both cases, apoptosis induction and caspase activation are consequences rather than the cause of delamination. Caspase activation is not detected even at the end of delamination induced by perturbation (Fig. S5*C*), and its inhibition by p35 expression does not suppress it (Fig. S5*D*). Indeed our results suggest that the suppressive effects of p35 on delamination previously observed (10) can be rescued by the addition of a mechanical stress.

The mechanoresponse we have delineated enables the extraction of quantitative dynamic signatures associated with different classes of regulatory molecules that can predict contributions of molecules to the physical constraints operating at cellular interfaces. Indeed our analysis of the integrin mutant is a good case in point. The flattening of the response at its summit correlates well with the actin reorganization defects we observe. Our analysis of the response on severing microtubules allows us to predict that the failure of microtubule reorganization may underlie delayed extrusion in these mutants.

Subcellular Stresses Patterning Delamination. Our work reveals that the response to both natural and induced delamination is local and does not extend beyond the nearest neighbors, implying a "screening" of elastic stresses. Further, it suggests that the dynamics of delamination in the AS is a consequence of both active cortical stresses arising from "line tension" and "cortical elasticity," as has been deemed sufficient to explain stable packing geometries (13, 14) and active cell-body stresses (15, 16, 37) generated by the remodeling of both the actomyosin and microtubule cytoskeletons we observe. Our experimental observations and theoretical proposal also suggest that differences in relative contributions of cell adhesion and active stresses must be instrumental in driving differences in tissue dynamics and pave the way for the mechanistic understanding of mechanosignaling in situ.

Conclusions

Our work has demonstrated that a mechanical stimulus can lead to the emergence of molecular polarities, generating polarized active stresses (at the cell surface and in the body) that drive shape transformations patterning cell delamination. It has also shown that the response to the mechanical stimulus can be modulated by surface adhesion and suggested that differences in adhesion may underlie differences in spatial patterns.

Materials and Methods

Fly Genetics. The *Drosophila* stocks UbiDE-Cadherin GFP (38) (from T. Uemura, Kyoto, Japan), Histone H2B EGFP, sqh GFP (39) (from J. Raff, Oxford, UK), and UAS-Apoliner (Bloomington Stock Center) were used to constitutively mark apical membranes at the level of adherens junctions, nuclei, nonmuscle myosin II RLC, and caspase activity, respectively. Recombinants of maternal α-tubulin Gal4 and UAS EB1GFP (III) (from D. St. Johnston, Cambridge, UK and T. Uemura, respectively) and armadilloGal4 and UAS α-catenin GFP (II) [from Bloomington Stock Center and H. Oda (40), respectively] were used to label microtubule (plus ends) and cell junctions respectively, in all cells. No differences in any of the parameters measured were detected between Ubi DE-Cadherin GFP and armadillo Gal4 and UAS α-catenin GFP. Microtubules were also visualized using the β-tubulin GFP protein trap [YC0063 GFP protein trap database (41)]. Actin was visualized using UAS actin5C GFP (Bloomington Stock Center) driven using c^{381}Gal4. For genetic perturbation experiments, UAS αPS3 integrin RNAi (VDRC), UAS βPS integrin RNAi (to down-regulate integrin adhesion and signaling in the AS; NIG), UAS spastin eGFP [to sever microtubules; from D. Brunner, Zurich, Switzerland (36)], and UAS p35 (Bloomington Stock Center) were used. A list of genotypes analyzed is provided in *SI Materials and Methods*.

Timed collections of embryos were made at 29 °C to enrich for stages 13–16. The embryos were dechorioniated in 50% bleach and mounted on a coverslip in halocarbon oil 700 (Sigma H8898).

Subcellular Laser Perturbation. Cells of the AS that are in the center of the ellipse were chosen for ablations. The laser radiation for ablation was generated in a titanium-sapphire laser system (Mai Tai Deep See HP; Spectra Physics) mounted on a Zeiss LSM 710 confocal microscope. A mode-locked oscillator delivers 80- to 100-fs pulse at a repetition rate of 80 MHz at a wavelength of 835 nm. The laser light is focused into the sample with a Plan-Neofluar 40× 1.3-N.A. oil-immersion objective. The laser power at the sample plane was 72 mW at a single spot. For ablation, a circular region approximately equal to the diffraction-limited spot is scanned for 40 iterations (pixel dwell of 6.04 μs). The region of ablation is cytoplasmic without perturbing the plasma membrane (2 μm basally from where E-Cadherin GFP signal first appears). For ablations in Figs. 2 and 3, the laser light (810 nm) was focused into the sample plane of a Plan-Neofluar 63× 1.4-N.A. oil-immersion objective. The laser power at the sample plane was close to 100 mW at a single spot. For ablation, a circular region approximately equal to the diffraction-limited spot was scanned for 20 iterations (pixel dwell time of 6.30 μs).

A list of genotypes analyzed and details regarding imaging, immunochemistry, and quantitative morphological analysis are given in *SI Materials and Methods*.

ACKNOWLEDGMENTS. We thank Drs. Nick Brown, Damian Brunner, Hiroki Oda, Jordan Raff, Daniel St. Johnston, Tadashi Uemura, and the Bloomington Stock Center for fly stocks; Dr. H. Krishnamurthy and the Central Imaging and Flow Facility [National Center for Biological Sciences (NCBS), Bangalore] for help with microscopy in the initial stages of this project; colleagues in the laboratories of M.N. and G.V.S. for support and lively discussions; Profs. Albert Libchaber, Satyajit Mayor, Roddam Narasimha, Veronica Rodrigues, and Apurva Sarin for comments on various versions of the manuscript; Prof. Veronica Rodrigues for encouragement and inspiration; and colleagues at NCBS, Bangalore, and Tata Institute of Fundamental Research (TIFR), Mumbai, for support. This work was supported by intramural funds from the Tata Institute of Fundamental Research (to M.N. and G.V.S.), the Department of Science and Technology Nanoscience Initiative (G.V.S.), and the Human Frontiers of Science Programme (M.R.).

1. Lecuit T (2005) Adhesion remodeling underlying tissue morphogenesis. *Trends Cell Biol* 15:34–42.
2. Juliano RL (2002) Signal transduction by cell adhesion receptors and the cytoskeleton: Functions of integrins, cadherins, selectins, and immunoglobulin-superfamily members. *Annu Rev Pharmacol Toxicol* 42:283–323.
3. Bershadsky AD, Balaban NQ, Geiger B (2003) Adhesion-dependent cell mechanosensitivity. *Annu Rev Cell Dev Biol* 19:677–695.
4. Vogel V, Sheetz M (2006) Local force and geometry sensing regulate cell functions. *Nat Rev Mol Cell Biol* 7:265–275.
5. Hutson MS, et al. (2003) Forces for morphogenesis investigated with laser microsurgery and quantitative modeling. *Science* 300:145–149.
6. Kiehart DP, Galbraith CG, Edwards KA, Rickoll WL, Montague RA (2000) Multiple forces contribute to cell sheet morphogenesis for dorsal closure in Drosophila. *J Cell Biol* 149:471–490.
7. Narasimha M, Brown NH (2004) Novel functions for integrins in epithelial morphogenesis. *Curr Biol* 14:381–385.
8. Peralta XG, et al. (2007) Upregulation of forces and morphogenic asymmetries in dorsal closure during *Drosophila* development. *Biophys J* 92:2583–2596.
9. Jacinto A, Woolner S, Martin P (2002) Dynamic analysis of dorsal closure in *Drosophila*: From genetics to cell biology. *Dev Cell* 3:9–19.
10. Toyama Y, Peralta XG, Wells AR, Kiehart DP, Edwards GS (2008) Apoptotic force and tissue dynamics during *Drosophila* embryogenesis. *Science* 321:1683–1686.
11. Mazumder A, Shivashankar GV (2007) Gold-nanoparticle-assisted laser perturbation of chromatin assembly reveals unusual aspects of nuclear architecture within living cells. *Biophys J* 93:2209–2216.
12. Kumar S, et al. (2006) Viscoelastic retraction of single living stress fibers and its impact on cell shape, cytoskeletal organization, and extracellular matrix mechanics. *Biophys J* 90:3762–3773.
13. Farhadifar R, Röper JC, Aigouy B, Eaton S, Jülicher F (2007) The influence of cell mechanics, cell-cell interactions, and proliferation on epithelial packing. *Curr Biol* 17: 2095–2104.
14. Rauzi M, Verant P, Lecuit T, Lenne PF (2008) Nature and anisotropy of cortical forces orienting *Drosophila* tissue morphogenesis. *Nat Cell Biol* 10:1401–1410.
15. Hatwalne Y, Ramaswamy S, Rao M, Simha RA (2004) Rheology of active-particle suspensions. *Phys Rev Lett* 92:118101–118104.
16. Lau AWC, Hoffman BD, Davies A, Crocker JC, Lubensky TCPRL (2003) Microrheology, stress fluctuations, and active behavior of living cells. *Phys Rev Lett* 91:198101–198104.
17. Heisterkamp A, et al. (2005) Pulse energy dependence of subcellular dissection by femtosecond laser pulses. *Opt Express* 13:3690–3696.
18. Clark AG, et al. (2009) Integration of single and multicellular wound responses. *Curr Biol* 19:1389–1395.
19. Hutson MS, et al. (2009) Combining laser microsurgery and finite element modeling to assess cell-level epithelial mechanics. *Biophys J* 97:3075–3085.
20. Mandato CA, Bement WM (2003) Actomyosin transports microtubules and microtubules control actomyosin recruitment during *Xenopus* oocyte wound healing. *Curr Biol* 13: 1096–1105.
21. Slattum G, McGee KM, Rosenblatt J (2009) P115 RhoGEF and microtubules decide the direction apoptotic cells extrude from an epithelium. *J Cell Biol* 186:693–702.
22. Mazumder A, Roopa T, Basu A, Mahadevan L, Shivashankar GV (2008) Dynamics of chromatin decondensation reveals the structural integrity of a mechanically prestressed nucleus. *Biophys J* 95:3028–3035.
23. Mayer M, Depken M, Bois JS, Jülicher F, Grill SW (2010) Anisotropies in cortical tension reveal the physical basis of polarizing cortical flows. *Nature* 467:617–621.
24. Kuhn SJ, Hallahan DE, Giorgio TD (2006) Characterization of superparamagnetic nanoparticle interactions with extracellular matrix in an in vitro system. *Ann Biomed Eng* 34:51–58.
25. Zhelev DV, Needham D, Hochmuth RM (1994) Role of the membrane cortex in neutrophil deformation in small pipets. *Biophys J* 67:696–705.
26. Wang N, et al. (2002) Cell prestress. I. Stiffness and prestress are closely associated in adherent contractile cells. *Am J Physiol Cell Physiol* 282:C606–C616.
27. Narasimha M, Brown N (2006) Integrins and associated proteins in Drosophila development. *Integrins and Development*, ed Danen E (Landes Bioscience, Austin, TX).
28. Giannone G, et al. (2007) Lamellipodial actin mechanically links myosin activity with adhesion-site formation. *Cell* 128:561–575.
29. Rosenblatt J, Raff MC, Cramer LP (2001) An epithelial cell destined for apoptosis signals its neighbors to extrude it by an actin- and myosin-dependent mechanism. *Curr Biol* 11:1847–1857.
30. Tamada M, Perez TD, Nelson WJ, Sheetz MP (2007) Two distinct modes of myosin assembly and dynamics during epithelial wound closure. *J Cell Biol* 176:27–33.
31. Paluch E, van der Gucht J, Sykes C (2006) Cracking up: Symmetry breaking in cellular systems. *J Cell Biol* 175:687–692.
32. Fernandez-Gonzalez R, Simoes SdeM, Röper JC, Eaton S, Zallen JA (2009) Myosin II dynamics are regulated by tension in intercalating cells. *Dev Cell* 17:736–743.
33. Yoshigi M, Hoffman LM, Jensen CC, Yost HJ, Beckerle MC (2005) Mechanical force mobilizes zyxin from focal adhesions to actin filaments and regulates cytoskeletal reinforcement. *J Cell Biol* 171:209–215.
34. Pouille PA, Ahmadi P, Brunet AC, Farge E (2009) Mechanical signals trigger Myosin II redistribution and mesoderm invagination in *Drosophila* embryos. *Sci Signal* 2:ra16.
35. Hirata H, Tatsumi H, Sokabe M (2008) Mechanical forces facilitate actin polymerization at focal adhesions in a zyxin-dependent manner. *J Cell Sci* 121:2795–2804.
36. Jankovics F, Brunner D (2006) Transiently reorganized microtubules are essential for zippering during dorsal closure in *Drosophila melanogaster*. *Dev Cell* 11:375–385.
37. Kruse K, Joanny JF, Julicher F, Prost J (2005) Generic theory of active polar gels: A paradigm for cytoskeletal dynamics. *Eur Phys J E Soft Matter* 16:5–16.
38. Uemura T, et al. (1996) Zygotic *Drosophila* E-cadherin expression is required for processes of dynamic epithelial cell rearrangement in the *Drosophila* embryo. *Genes Dev* 10:659–671.
39. Royou A, Sullivan W, Karess R (2002) Cortical recruitment of nonmuscle myosin II in early syncytial *Drosophila* embryos: Its role in nuclear axial expansion and its regulation by Cdc2 activity. *J Cell Biol* 158:127–137.
40. Oda H, Tsukita S (1999) Dynamic features of adherens junctions during *Drosophila* embryonic epithelial morphogenesis revealed by a Dalpha-catenin-GFP fusion protein. *Dev Genes Evol* 209:218–225.
41. Morin X, Daneman R, Zavortink M, Chia W (2001) A protein trap strategy to detect GFP-tagged proteins expressed from their endogenous loci in *Drosophila*. *Proc Natl Acad Sci USA* 98:15050–15055.